Working Paper

Land-Use and Land-Cover Mapping of Getik River Basin, Armenia

Aghavni Harutyunyan[1], Stefan Schlaffer[1,2], Thi Ngoc Han Nguyen[3], Artak Piloyan[4]

[1]AUA Acopian Center for the Environment, American University of Armenia
[2]German Aerospace Center
[3]University of Hohenheim
[4]Yerevan State University Faculty of Geography and Geology

April 25, 2019

This project is a part of the DAAD-funded collaboration, GAtES (German-Armenian Network on the Advancement of Public Participation GIS for Ecosystem Services as a Means for Biodiversity Conservation and Sustainable Development), between the University of Hohenheim (UHOH) and the American University of Armenia's (AUA) Acopian Center for the Environment.

1. Introduction

The mapping of Land Use and Land Cover (LULC) changes has a crucial role for a better understanding of the processes on Earth, such as land productivity, carbon emissions and storage, biodiversity, the biogeochemical and hydrological cycles. The modeling, monitoring and assessing of land cover characteristics and resources is also important for detecting the changes in the ecosystem and their consequences (Giri, 2012). LULC maps or models help to observe human-environment dynamics that produce changes in the environment (Lambin et al., 2003).

Armenia is one of the global hot-spots of biodiversity. But the rich natural capital is under a multitude of anthropogenic pressures originating from mining, livestock farming, logging, water overuse, and more. Forests and pastures are particularly affected. Degradation of these ecosystems goes along with a loss of ecosystem services, including provisioning (e.g. timber, food, medicines), regulating (e.g. water storage, erosion control) and cultural services (e.g. cultural heritage, ecotourism). However, there is currently no nation-wide LULC product available showing the current situation.

Due to the remoteness and size of the areas of interest, remote sensing-based methods have been used since the 1970s for mapping LULC. With the steadily growing amounts of earth observation (EO) data, methods have been more and more automated.

To monitor and evaluate the mentioned problems, LULC mapping project was counted using remotely sensed imagery in the Getik Valley (Figure 1) including both optical and Radar data. Freely available Sentinel-1 and Sentinel-2 data from the Copernicus program were used, which are jointly operated by the European Space Agency (ESA) and the European Commission. The data are available from the Copernicus Open Access Hub[1].

The main goal of this study is to provide a detailed LULC map, which will help to understand current land cover conditions in the study area and how it is being used by communities, which will serve as a starting point for monitoring changes over time. The map can also be a good basis of further environmental research projects, as well as an important source of information for land management and land planning activities.

The applied methods and materials with the information about study area, used datasets, as well as data processing and classification methods are described in section 2. The results and discussion are introduced in section 3, and the conclusion is given in section 4.

The research project is a part of the DAAD-funded collaboration “German-Armenian Network on the Advancement of Public Participation GIS for Ecosystem Services as a Means for Biodiversity Conservation and Sustainable Development (GAtES)”[2] between the University of

[1] https://scihub.copernicus.eu/
[2] http://ace.aua.am/gates

Hohenheim and the American University of Armenia Acopian Center for the Environment. GAtES harnesses the ecosystem services framework and Public Participation GIS (PPGIS) methods for enhancing biodiversity conservation and sustainable development in Armenia.

2. Methods and Material

2.1. Study area

The study area of this project is the Getik River Basin located in north-eastern part of Lake Sevan (Figure 1). Getik Valley is situated between the mountain ranges of Miapor and Areguni, through which runs the river with the same name. The catchment area is 581 km^2. Elevation ranges between 898 m and 2985 m. The largest community is Chambarak with a population of 5,652. Overall, there are 14 settlements in the study area and the total population is 12,549 as of January 1, 2018 (Statistical Committee of the Republic of Armenia[3]).

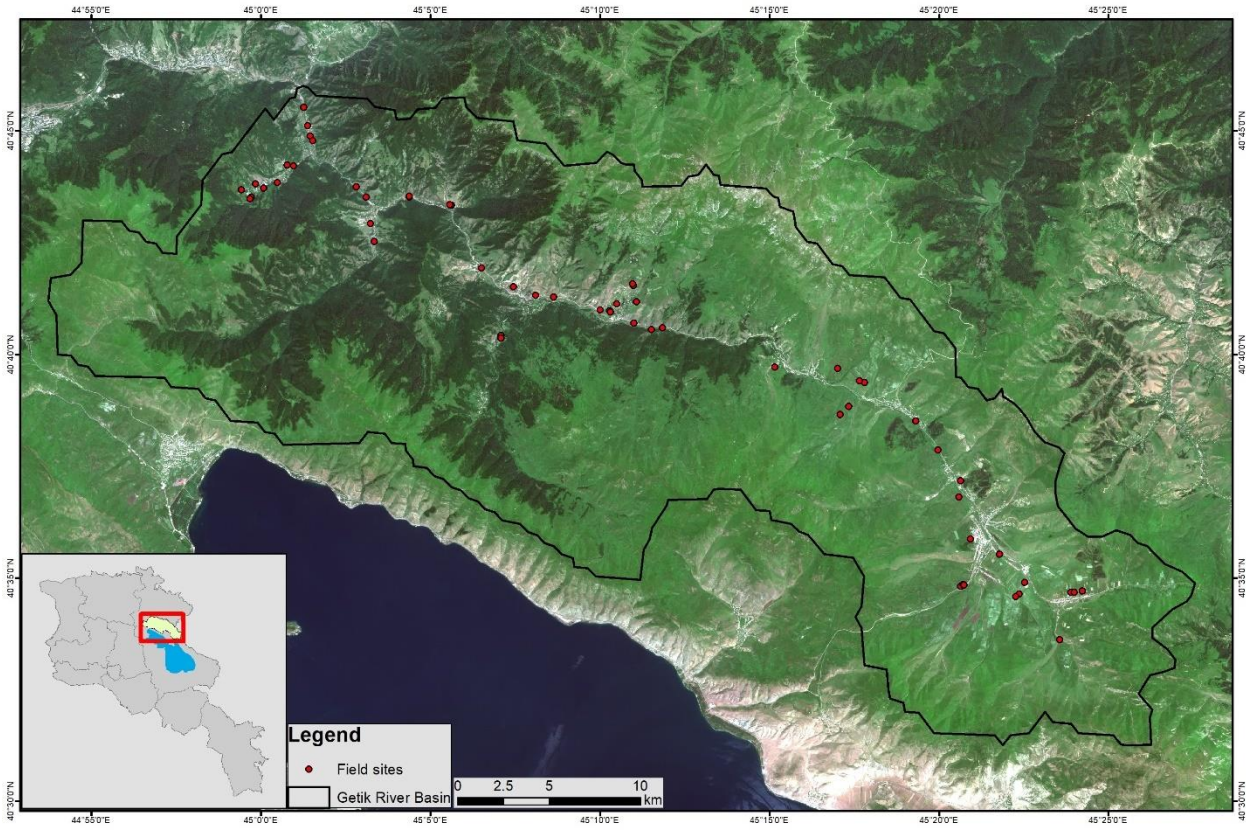

Figure 1: Natural-color RGB composite (R: Red, G: Green, B: Blue channel) of Sentinel-2B image covering the study area. The inset shows the location of the study area within Armenia.

[3] https://www.armstat.am

2.2. Datasets

2.2.1. Satellite data

Data from the Copernicus Sentinel-1 (SAR) and Sentinel-2 (optical) missions were used for LULC classification. The used datasets with their acquisition date and time, as well as orbit directions are shown in Table 1. All the images were acquired between July and beginning of October 2018.

Three Sentinel-2B MSI (Multi Spectral Instrument) were chosen for image classification. The Sentinel-2 mission measures the Earth's reflected radiance in 13 spectral bands, spanning from the visible and the near infrared to the short wave infrared, and the spatial resolution varies from 10 m to 60 m (Spoto et al., 2012). The data obtained from Sentinel-2 were combined with information obtained from Sentinel-1, in order to receive the final LULC map.

Eight Sentinel-1A Single Look Complex (SLC) images were used for mapping built-up in Getik Valley. The Sentinel-1 mission is a two-satellite constellation, which offers six days exact repeats over Europe (Torres et al., 2012). Since the scattering properties of buildings depend on their orientation with respect to the viewing geometry of the radar sensor, acquisitions from different angles have to be combined for built-up area mapping. Therefore, data received from descending and ascending orbit directions were processed and combined. The processing steps of both optical and SAR data are introduced in the subsection 2.3.

Table 1: Satellite datasets used as input data for the LULC classification.

Satellite and sensor	Acquisition date/time	Orbit direction	Tiles	Cloud cover (%)
Optical data				
Sentinel-2B MSIL2A	01.07.2018 07:46:09 UTC	Descending	38TNK	7.2
Sentinel-2B MSIL2A	01.07.2018 07:46:09 UTC	Descending	38TML	0.4
Sentinel-2B MSIL2A	01.07.2018 07:46:09 UTC	Descending	38TNL	0.0
SAR data				
Sentinel-1A IW SLC	21.08.2018 14:53:32 UTC	Ascending		
Sentinel-1A IW SLC	02.09.2018 14:53:32 UTC	Ascending		
Sentinel-1A IW SLC	14.09.2018 14:53:32 UTC	Ascending		
Sentinel-1A IW SLC	26.09.2018 14:53:32 UTC	Ascending		
Sentinel-1A IW SLC	01.09.2018 03:08:38 UTC	Descending		
Sentinel-1A IW SLC	13.09.2018 03:08:38 UTC	Descending		
Sentinel-1A IW SLC	25.09.2018 03:08:38 UTC	Descending		
Sentinel-1A IW SLC	07.10.2018 03:08:39 UTC	Descending		

2.2.2. Field work and data

Field work was conducted to procure in-situ data for validation and training of the classification approach. The ground truthing work was conducted on three different days in September 2018. The study area was divided into three parts: northern, central, and southern, and each day we

were working in one of the parts. We visited the areas that were unclear from the initial analysis and checked via the ground truthing process. The locations of ground truthing areas are shown in Figure 1. In addition, we also used a drone (DJI Phantom 3 Pro equipped with a Canon 12MPixel camera) to investigate remote areas difficult to reach by foot or car (e.g. Figure 2a and 2b). In total, 70 sites were visited.

The collected data were used to define the training areas for supervised classification applied to Sentinel-2 scene. The data were also used for assessing the accuracy of the classification. Some of the photos taken during our visit (including drone photos) are shown in Figure 2.

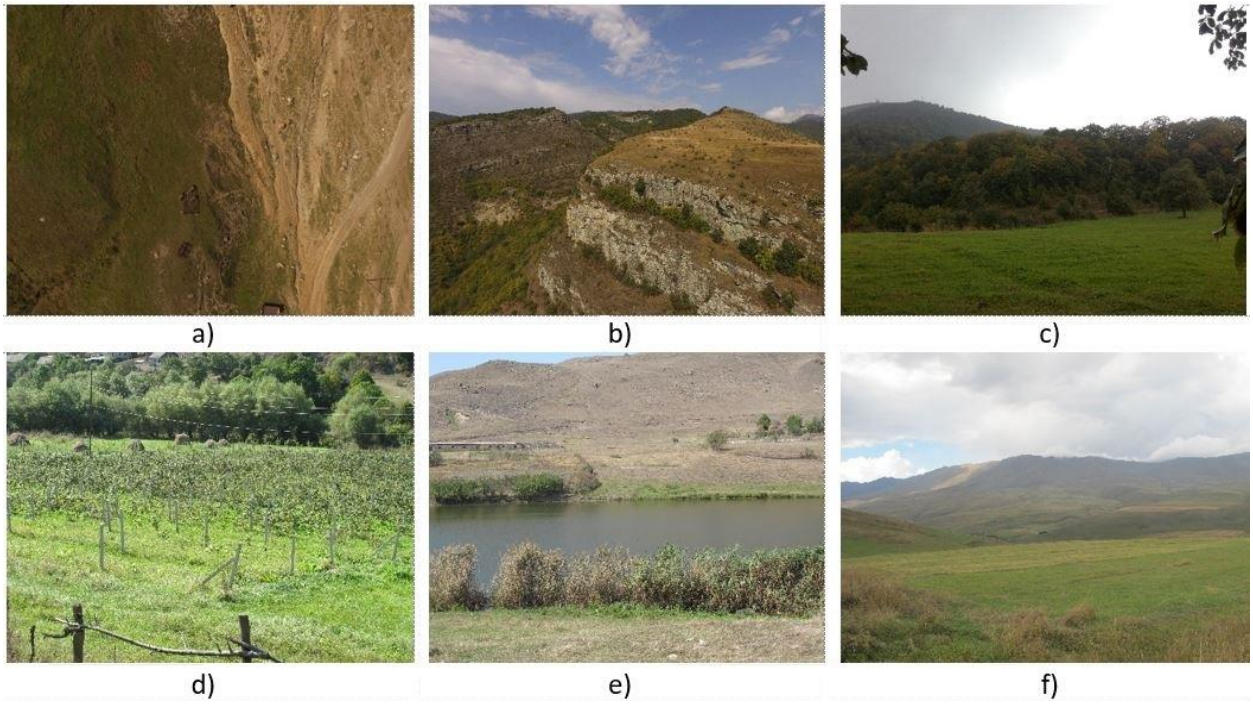

Figure 2: a) Grassland and bare area (Drone photo), b) Bare rocks and sparse shrub lands on the slopes (Drone photo), c) Grassland and forest in the background, d) Agricultural area, e) Open water, f) Pasture and grassland.

2.2.3. Ancillary datasets

Terrain slope and elevation were used in the applied rule-based classification for obtaining built-up areas. Additionally, slope data was also used for constraining the classification of agricultural areas. The 30 m spatial resolution digital elevation model (DEM) from Shuttle Radar Topography Mission (SRTM)[4] were used in this study. A vector data of Catchment areas is available on the website of the AUA Acopian Center for the Environment[5], which was used for identifying the boundaries of Getik River Basin.

[4] https://www2.jpl.nasa.gov/srtm/
[5] https://ace.aua.am/gis-and-remote-sensing/vector-data/

2.3. Data processing

The Sentinel Applications Platform (SNAP, version 6.0) and ESRI ArcGIS 10.1 were used for data processing and visualization.

2.3.1. Optical data processing

The Sentinel-2 satellite image (Level-2A) was downloaded from ESA's Sentinel Data Hub. The Level-2A product provides Bottom of Atmosphere reflectance images derived from the Level-1C products (Djamai and Fernandes, 2018). After resampling the images (3 tiles), they were mosaicked and the subset image was created (Figure 1), which was used for classification.

2.3.2. Synthetic Aperture Radar (SAR) data processing

A Synthetic Aperture Radar (SAR) is a space-borne side-looking radar system which relies on the flight path to simulate an extremely large antenna or aperture electronically (Hopkins, 2018).

The Sentinel-1 mission consists of a constellation of two satellites, which share the same orbital plane with ascending and descending flight directions. Due to this, the same area can be scanned from two different geometric sides. The ascending orbit is when the satellite travels from south to north over the Earth's surface and views the target area from the western flank, and the descending orbit is when the satellite travels from north to south and views the target area from the eastern flank (Mora et al., 2016). This advantage of Sentinel-1 mission was used for delineating built-up areas.

The dataset used as input data is shown in Table 1. The algorithm which was used for getting the built-up data is based on two main parameters: Backscattering intensity (Gamma naught) and InSAR Coherence, as built-up areas are coherent in time and have high backscatter coefficient (Chini et al., 2017). The Sentinel Application Platform (SNAP, version 6.0) was used for SAR data processing.

The processing chain for estimating interferometric coherence between a pair of Sentinel-1 Single-Look Complex (SLC) scenes is shown in Figure 3.

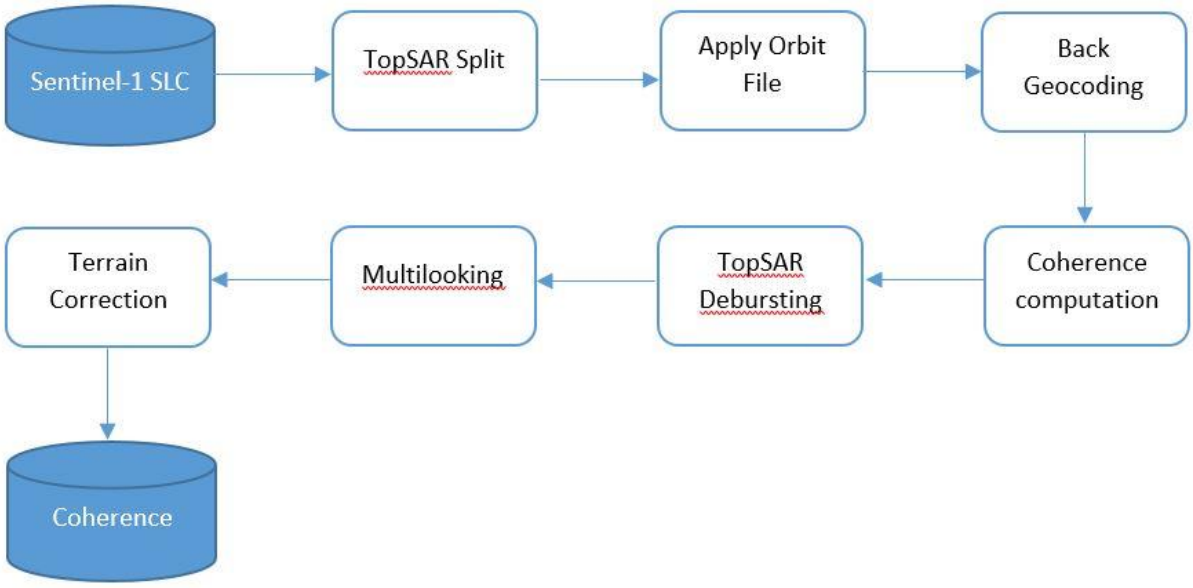

Figure 3: Processing chain for geocoded Coherence applied to Sentinel-1 SLC datasets.

First, the images were split in order to get the separate subswath and bursts covering the study area and then the Apply Orbit File operator was used, which provides accurate satellite position and velocity information. Then, the image pairs were co-registered using Back Geocoding operator, and after that the Coherence image was computed using a window of 10 x 3 pixels.

The coherence image was debursted using the TopSAR Debursting operator and then, in order to obtain square pixels, the coherence images were multilooked, as a post-processing step. Terrain effects were corrected using the Range-Doppler algorithm for compensating all geometric distortions of the image. Additionally, to account for the radiometric effects of terrain, a radiometric terrain correction was applied to each image (Small, 2011).

The obtained coherence maps between image pairs for descending path are shown in Figure 4 both for VV and VH polarizations. The image derived from September 1st, 2018 was used as a master image.

The final coherence images (both for ascending and descending paths) were created by averaging coherence over all images for each orbital node (i.e. ascending and descending).

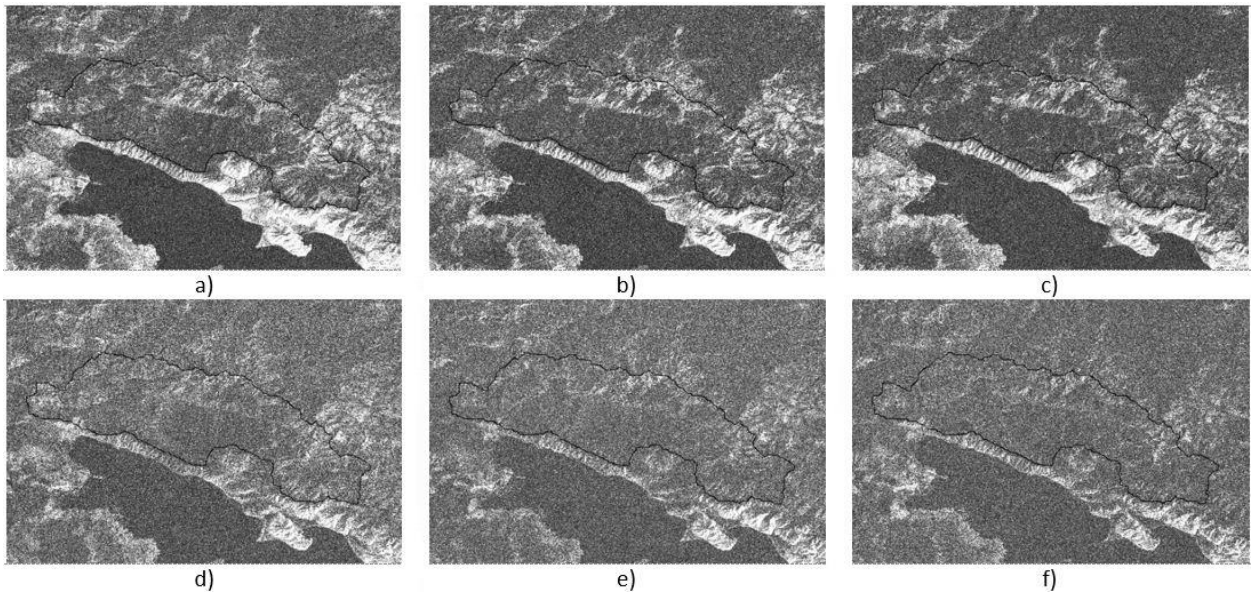

Figure 4: Coherence maps of study area for a descending path of Sentinel-1: a) Image pairs of 01-Sep-2018 and 13-Sep-2018 for VV polarization, b) Image pairs of 01-Sep-2018 and 25-Sep-2018 for VV polarization, c) Image pairs of 01-Sep-2018 and 07-Oct-2018 for VV polarization, d) Image pairs of 01-Sep-2018 and 13-Sep-2018 for VH polarization, e) Image pairs of 01-Sep-2018 and 25-Sep-2018 for VH polarization, f) Image pairs of 01-Sep-2018 and 07-Oct-2018 for VH polarization. The black line shows the location of the study area within Armenia.

The processing chain to obtain the backscattering intensity (gamma-naught) based on Sentinel-1 Single-Look Complex (SLC) is shown in Figure 5. The TopSAR Split and the Apply Orbit File operators were also used in processing chain applied for obtaining gamma-naught. Then, the Termal Noise Removal operator was applied.

For debursting and merging the image per swath and for reducing the speckle noise the following operators were applied: TopSAR Debursting, Multilooking and Speckle Filter. After filtering the images, terrain flattening gamma-naught was obtained with the help of a digital elevation model (DEM), which was then transformed to dB scale by applying equation 1:

$$\gamma^0[dB] = 10\ \log_{10}(\gamma^0[lin]). \qquad \text{(eq. 1)}$$

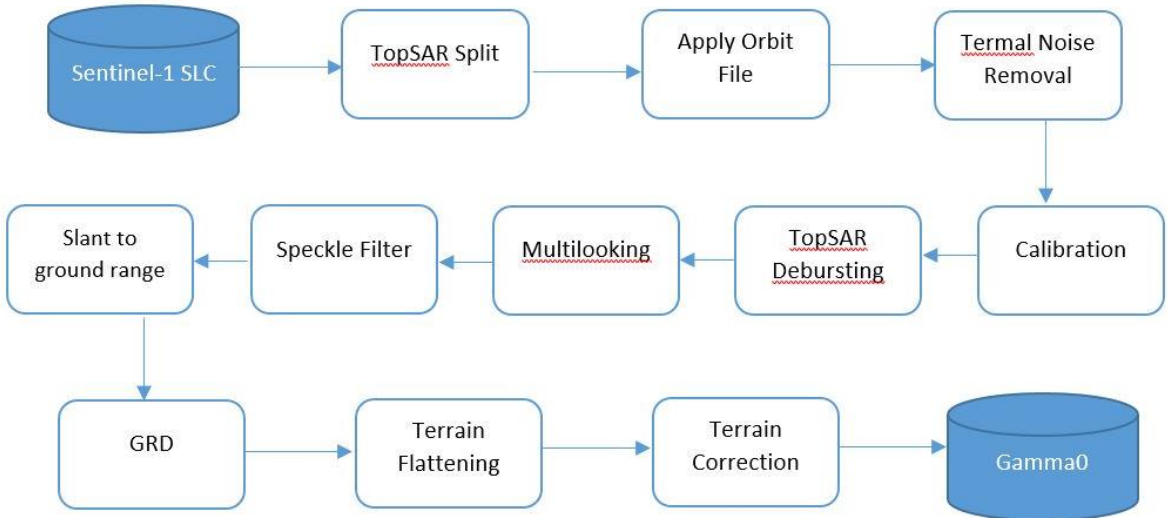

Figure 5: Processing chain for backscattering intensity applied to Sentinel-1 SLC datasets.

The maps as the results of the mentioned processing in Figure 5 are shown in Figure 6 only for descending path. After obtaining the gamma-naught images then they were averaged to obtain the final average backscattering coefficient both for ascending and descending paths.

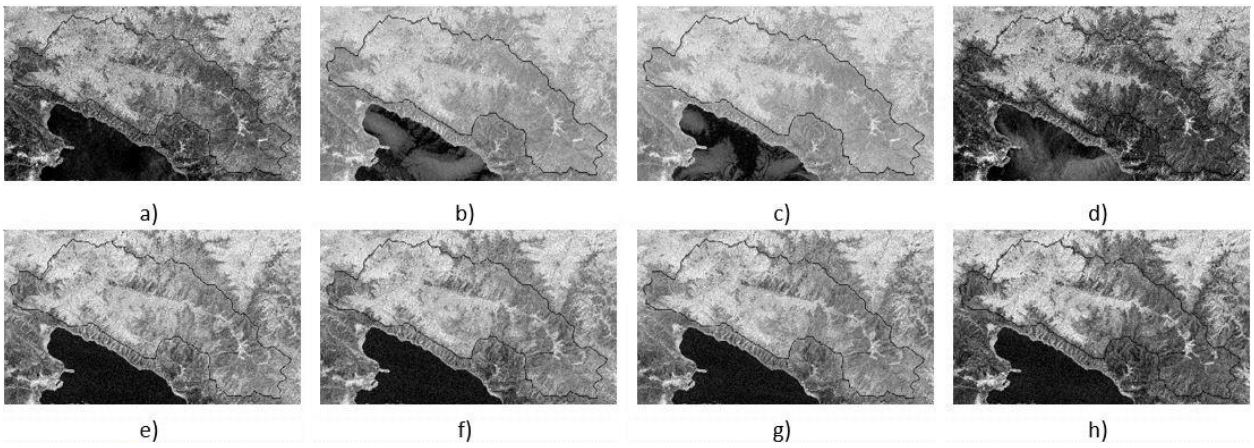

Figure 6: Backscattering intensity maps of study area for a descending path of Sentinel-1: a) Image of 01-Sep-2018 for VV polarization, b) Image of 13-Sep-2018 for VV polarization, c) Image of 25-Sep-2018 for VV polarization, d) Image of 07-Oct-2018 for VV polarization, e) Image of 01-Sep-2018 for VH polarization, f) Image of 13-Sep-2018 for VH polarization, g) Image of 25-Sep-2018 for VH polarization, h) Image of 07-Oct-2018 for VH polarization. The black line shows the location of the study area within Armenia.

2.3.3. Limitations of Optical and Radar Products

Both Optical and Radar data have limitations. The first limitation of optical data encountered in this study relates to similar spectral signatures of different LULC classes (Joshi et al., 2016). This is mainly referring to agricultural classes, such as permanent crops (vineyards, fruit trees) and

heterogeneous agricultural areas. Second, urban (built-up) areas present a high variance of reflectance in optical images, which can lead to false detection (Corbane et al., 2008).

The major limitation of SAR product was due to topography, since the study area is mountainous. This limitation is connected to geometric and radiometric effects, such as radar shadow (Joshi et al., 2016).

2.4. Image classification

The Random Forest (RF) supervised classification approach was used for image classification (Breiman, 2001). A total of 277 training polygons was created based on ground truthing data and visual inspection of high-resolution and very-high-resolution satellite imagery available on Google Earth. Since the Google Earth imagery had a high percentage of cloud cover for the study area, we also used high-resolution imagery provided by Planet Labs (e.g. PlanetScope, RapidEye). Planet Labs data were made available as part of a research and education license (Planet Team, 2017). We applied the RF classification algorithm with 5000 training samples, and the number of trees was 500.

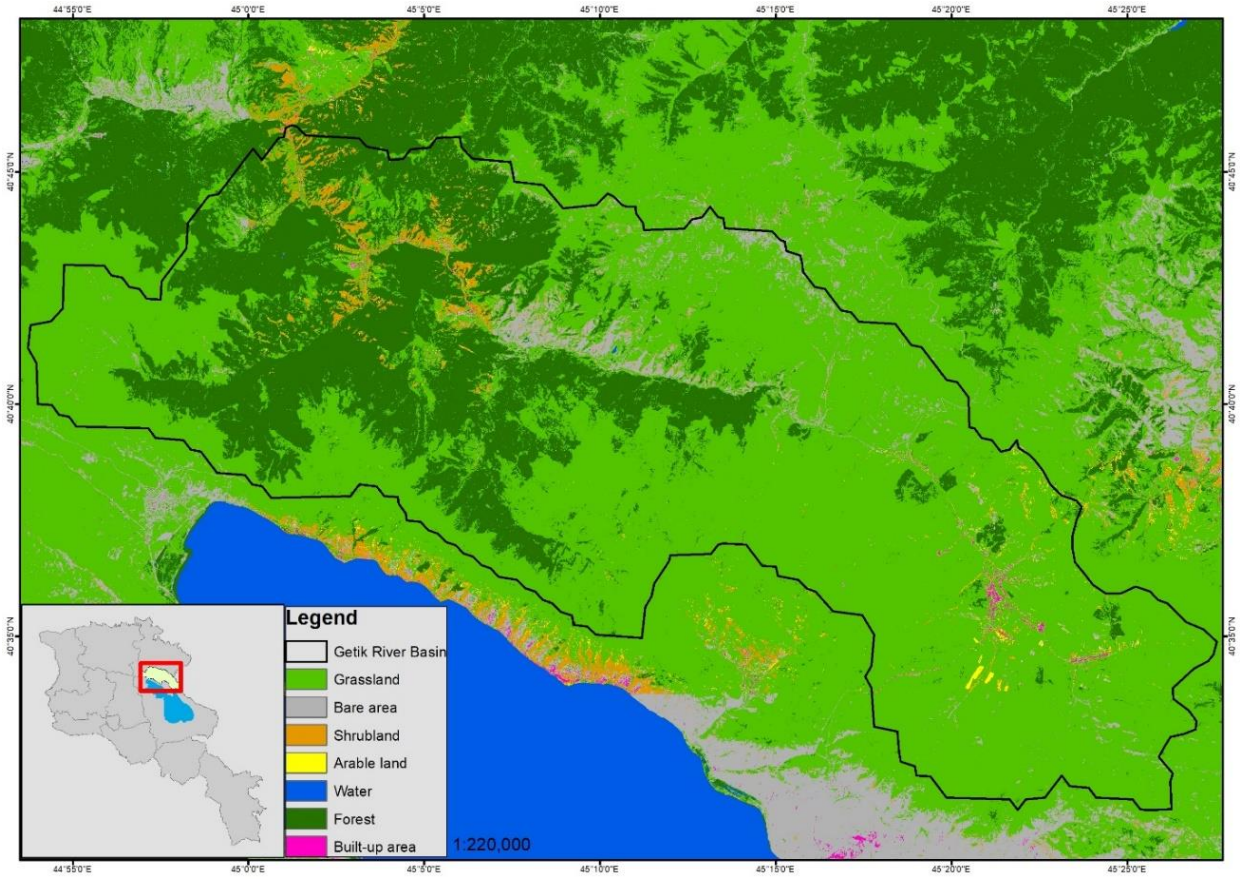

Figure 7: Preliminary LULC map of Getik river basin and its surrounding areas.

The classification result is shown in Figure 7. The preliminary LULC map has the following classes based on CORINE Land Cover nomenclature (Büttner et al., 2002): grassland, bare area, shrubland, arable land, water, forest and built-up area.

The Figure 8 is showing the reflectance values for each LULC classes. Forest and grassland have low reflectance values in the visible spectrum (492-664 nm) and high values in the near infrared (NIR) range of wavelengths (832 nm) (MSI Overview, Sentinel Online). The built-up areas and bare areas, which refers to the areas with sparse vegetation cover or stony areas, have some similarities of reflectance values that may cause confusion between them. To get rid of this confusion and to obtain accurate built-up areas, SAR data was used. As already mentioned, two main parameters of SAR data were used for mapping built-up areas: Backscatter coefficient gamma-naught and interferometric coherence.

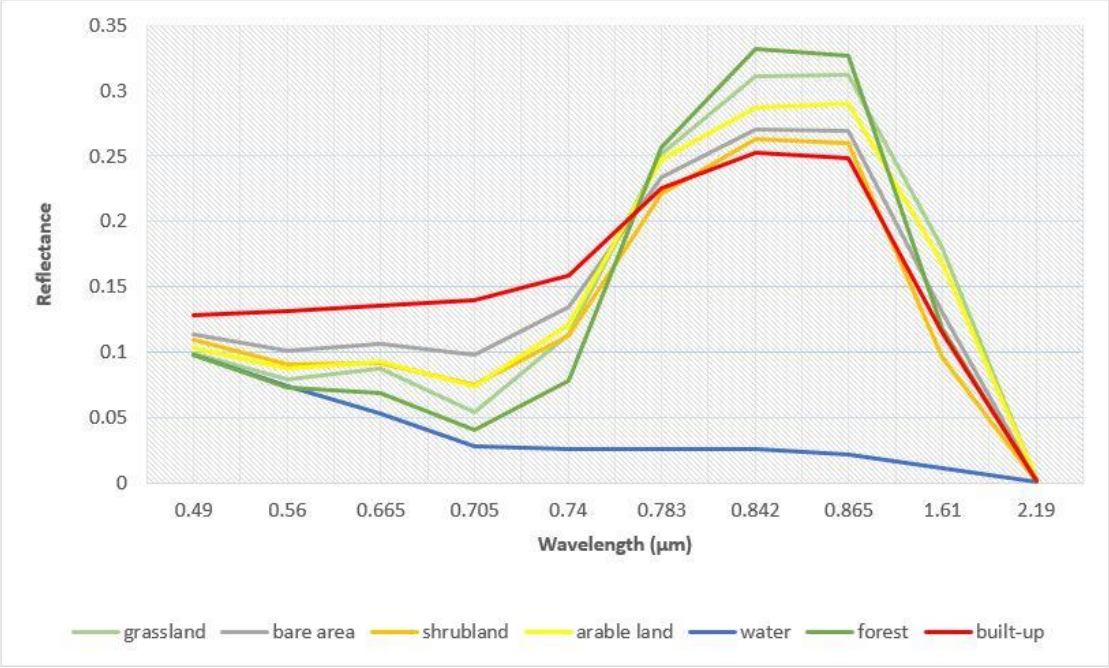

Figure 8: The average reflectance values for each LULC class.

The areas with high coherence appear bright in Figure 4. High coherence indicates that there are no random changes occurring between image acquisitions. Areas with high coherence mainly correspond to urban and bare areas. Therefore, they can be easily confused with urban areas. Low coherence is mainly caused by vegetation as small movements of twigs and leaves will lead to decorrelation between two image acquisitions. Further factors causing decorrelation include changes in atmospheric constituents, such as water vapor, or changes in soil moisture.

Manmade scatterers appear bright in the Backscattering intensity maps (Figure 6). Dihedral scatterers (e.g. the corners formed by buildings) are bright and have high values. Thus, the bright pixels in the maps correspond to areas of backscattered radiation (e.g. urban areas),

whereas dark pixels correspond to low backscattered radiation (e.g. water bodies), since the radiation of flat scatterers in general mirrored away from the satellite (InSAR Principles: Guideline, 2007). Water bodes appear mostly black in the intensity images.

Table 2: The parameters and the rules for built-up area classification.

Parameters	**Rule**	
	Ascending	**Descending**
Gamma0	> -9 dB	> -9 dB
Coherence	> 0.5	> 0.55
Slope	< 13°	< 12°
Elevation	< 2000 m	< 2000 m

To exploit the mentioned parameters jointly, rule-based classification was applied. The parameters and the rules, which were found based on trial and error, are shown in Table 2 for ascending and descending paths separately. The slope and the elevation data were also used in the rule. The preliminary result of rule-based classification is shown in Figure 9. After applying a majority filter (3-by-3 window), the final built-up data were added to the LULC map.

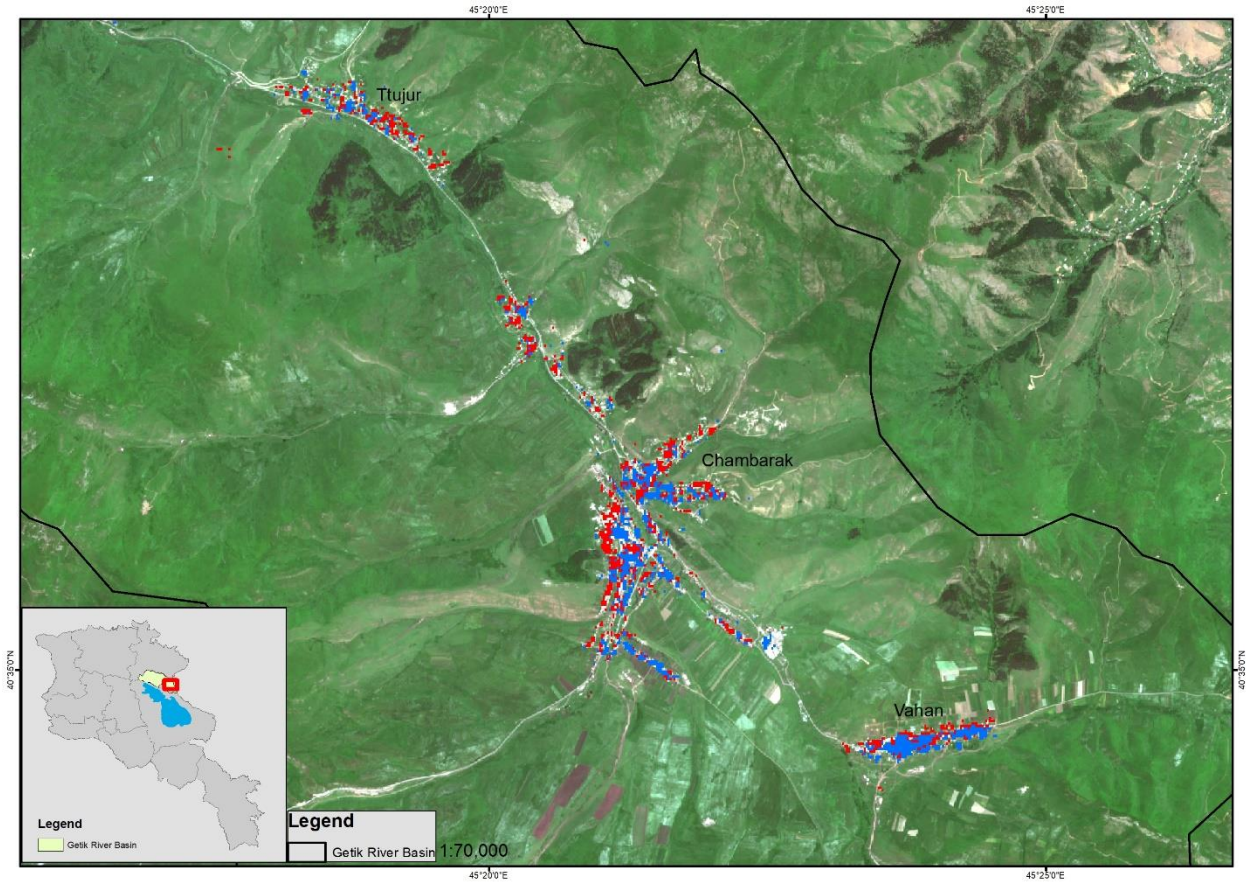

Figure 9: Built-up areas of the southern part of the Getik Valley obtained from Sentinel-1 images both for ascending (red pixels) and descending paths (blue pixels). Background image: Sentinel-2B.

In addition to the aforementioned LULC classes, a wetland class was added to the final map. These areas were identified during the field campaign, since it was difficult to find out the exact places on satellite images due to their small sizes. We created the wetland polygons manually using surveyed GPS coordinates and added them to the final LULC map.

2.5. Accuracy assessment

To assess the quality of data derived from satellite imagery, an accuracy assessment was conducted. The reference dataset used for accuracy assessment is based on ground truth data collected in the field, as well as data derived from high-resolution imagery (Google Earth, PlanetScope, RapidEye). The number of accuracy assessment points is 125, which was used to compile the confusion matrix using R programming language. The confusion matrix (Table 3) was used to calculate the overall accuracy of the classification, as well as its user's accuracies (error of commission) and producer's accuracies (error of omission). Overall accuracy shows the percentage of correctly classified pixels. Producer's accuracy shows the percentage of reference pixels that were correctly classified. User's accuracy represents the probability that a pixel labeled as a certain LULC class belongs to the same class in the reference dataset (Congalton and Green, 2008).

3. Results and Discussion

3.1 Field visit

Most of the visited sites are located in the surrounding areas of the settlements. It was difficult to distinguish arable lands from grasslands for many of the sites. Because of the lack of irrigation systems, many arable lands turned into grasslands (Harutyunyan, 2019). Since, the LULC map should represent the current land-use and land-cover, these kinds of areas were classified as grassland (Figure 10).

During the field visits, we identified wetlands (in the village of Aygut), which were difficult to determine from satellite images due to their small sizes.

Figure 10: Arable lands turned into grasslands

3.2 LULC classification

The final LULC map combining information derived from optical and SAR images is shown in Figure 11.

The final map consists of eight LULC classes: Grassland (including both natural grassland and pasture), Bare areas, Shrubland, Water bodies, Forest, Agriculture, Built-up areas and Wetlands.

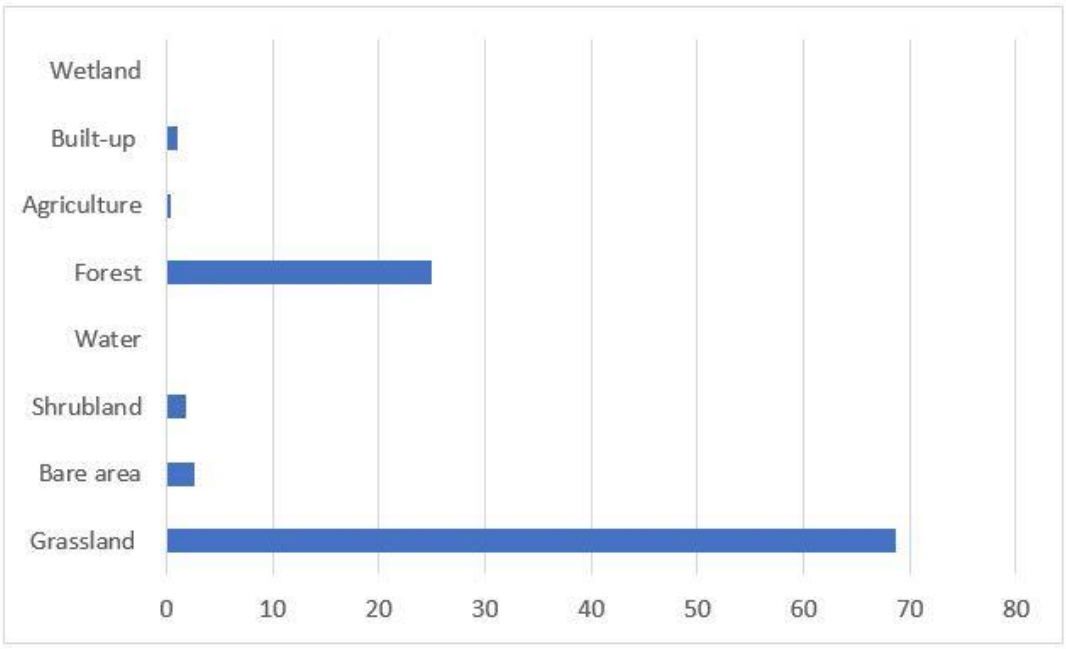

Figure 11: Summary of LULC classes given in %.

The percentage of each LULC class covering the study area is shown in Figure 10. According to that, the catchment is predominantly (68.6%) covered by Grassland and Pasture. They mainly cover the Southern part of the river basin and the areas at higher elevations (> 1800 m). Forest covers 25% of the study area and is mainly distributed over the Northern part. Shrubland (1.9%)

is also mainly located in the Northern part of the Getik Valley and mainly covers the slopes of the valley. The Eastern slopes of the valley located in the central part of the river basin were classified as bare areas (2.7%). Bare areas comprise open spaces with sparse vegetation cover and bare rocks. Roads are also classified as bare areas. Built-up areas make up 1% of river basin, and the open water and wetlands cover less than 1% of the study area. Agricultural areas also cover less than 1%. This class includes arable lands, permanent crops (vineyards, fruit trees) and heterogeneous agricultural areas, since it was difficult to distinguish them, connected to limitations already mentioned.

The confusion matrix of the comparison between the classification and the "ground-truth" samples is shown in Table 3. The overall accuracy of the map is 84%. The confusion matrix also shows the user's accuracy (UA) and the producer's accuracy (PA) for each class.

The overall accuracy is the sum of the correctly classified sample units (105) divided by the total number of sample units in the entire confusion matrix. As mentioned, the number of validation points is 125.

Basically, most of the land cover classes with high level of vegetation cover have high UA and PA (forest, grassland and pasture, shrubland). The highest value was obtained for water classe (100 % accuracy both for UA and PA), however, it covers a very small total area. The water class has low reflectance values across the bands covered by Sentinel-2 (Figure 8), and there is no confusion with the other classes. The class of agriculture has the lowest PA value (47%), the UA value is also low (64%). As indicated before, many agricultural areas have been converted into grasslands due to the lack of irrigation systems. This causes an additional confusion between those classes, but despite this fact, it is hard to distinguish agricultural areas and grasslands, even in high resolution imagery. UA is also low for the class of bare area, and the confusion is mainly connected to grassland and agriculture classes. Built-up areas have high accuracy (UA is 100% and PA is 82%). As described in subsection 2.3, Sentinel-1 data were used for delineating built-up areas and the result was added to the final map derived from Sentinel-2 data using supervised classification.

As already mentioned, the wetland class was mapped manually, using GPS data, and then was combined with the final map. Thus, the wetland class is not included in the table showing classification accuracies (Table 3).

Table 3: Classification accuracies of LULC map class with user's and producer's accuracies

	Grassland	Bare area	Shrubland	Water	Forest	Agriculture	Built-up	User's accuracy (%)
Grassland	48	1	1	0	0	4	0	87
Bare area	3	10	1	0	0	2	1	59
Shrubland	0	0	14	0	0	2	0	88
Water	0	0	0	3	0	0	0	100
Forest	0	0	0	0	14	0	0	93
Agriculture	2	1	0	0	0	7	1	64
Built-up	0	0	0	0	0	0	9	100
Producer's accuracy (%)	88	83	88	100	93	47	82	84

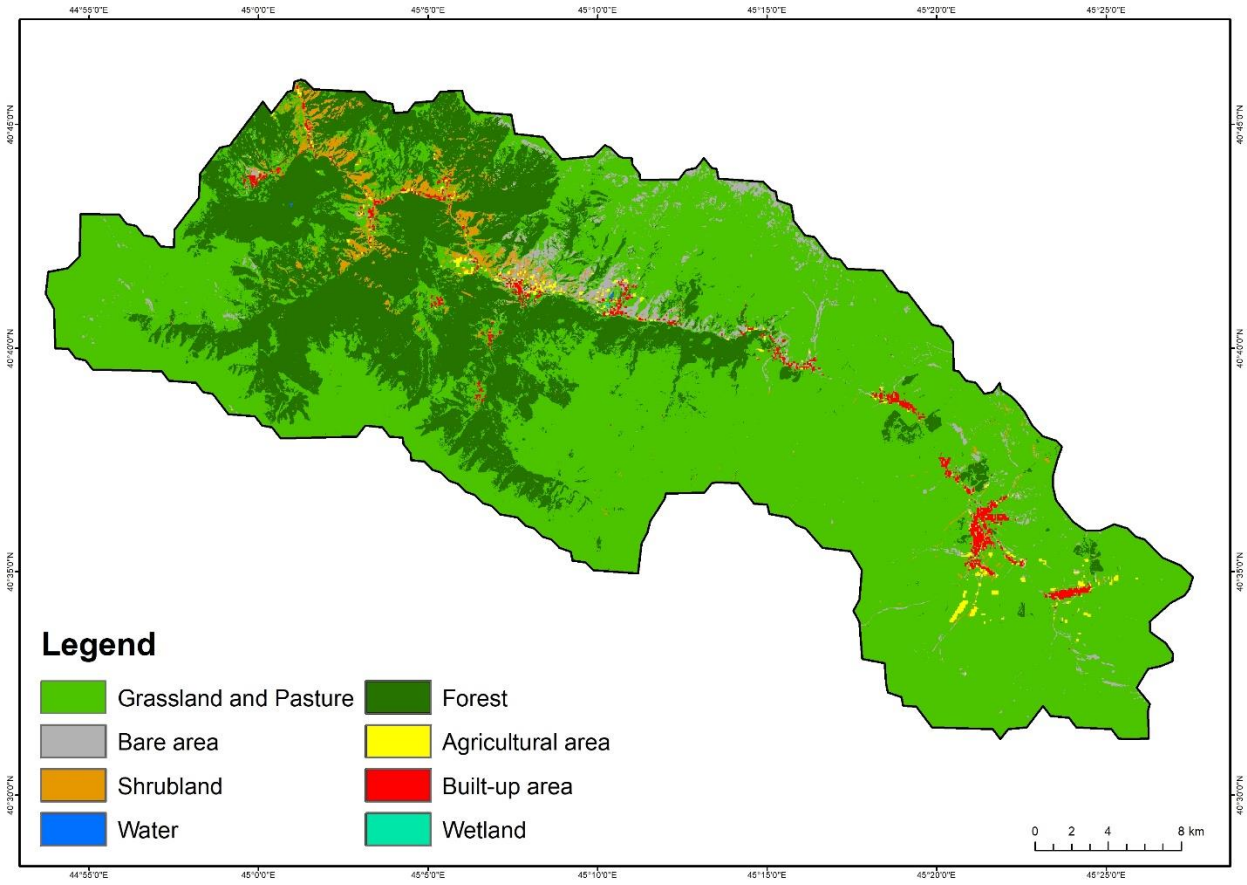

Figure 12: Final LULC map of Getik Valley.

4. Conclusion

This project was conducted to derive an accurate and detailed LULC map of the Getik River Valley since LULC mapping has a significant role for different environmental studies, which are currently being carried out or planned in the study area.

To achieve the best result, both Sentinel-1 and Sentinel-2 data were used and the final map is a combination of the data received from them separately. Although, both used datasets have specific limitations resulting in some challenges for mapping process. However, most of them do not have overlaps and basically complement each other. The classification procedure used in this study was able to distinguish eight LULC classes with an overall accuracy of 84%.

The map can be used in future studies for land use and land cover change detection analysis. It also can serve as an important source for land management and land planning activities.

5. Acknowledgments

This research project is a part of the DAAD-funded collaboration GAtES project between the University of Hohenheim and the American University of Armenia Acopian Center for the Environment. The satellite images used as an input data were provided by the Copernicus programme.

6. References

Breiman, L. (2001). Random forests. Machine learning, 45(1), 5-32.

Büttner, G., Feranec, J., Jaffrain, G., Steenmans, C., Gheorghe, A., & Lima, V. (2002). Corine land cover update 2000. Technical guidelines.

Chini, M., Pelich, R., Hostache, R., & Matgen, P. (2017). Built-up areas mapping at global scale based on adapative parametric thresholding of Sentinel-1 intensity & coherence time series. In Analysis of Multitemporal Remote Sensing Images (MultiTemp), 2017 9th International Workshop on the (pp. 1-4). IEEE.

Congalton, R. G., & Green, K. (2008). Assessing the accuracy of remotely sensed data: principles and practices. CRC press.

Corbane, C., Faure, J. F., Baghdadi, N., Villeneuve, N., & Petit, M. (2008). Rapid urban mapping using SAR/optical imagery synergy. Sensors, 8(11), 7125-7143.

Djamai, N., & Fernandes, R. (2018). Comparison of SNAP-derived Sentinel-2A L2A product to ESA product over Europe. Remote Sensing, 10(6), 926.

Giri, C. (Ed.). (2012). Remote Sensing of Land Use and Land Cover. Boca Raton: CRC Press, https://doi.org/10.1201/b11964

Harutyunyan, A., Pfeiffer, P., Vardanyan, K., Mamyan, M. (2019). Public Participation GIS for Mapping Land Use Patterns in Getik Valley. Working Paper. AUA Acopian Center for the Environment, American University of Armenia

Hopkins, M., (2018). Introduction to Remote Sensing, Syrawood Publishing House

InSAR Principles: Guidelines for SAR Interferometry Processing and Interpretation (TM-19, February 2007)

Joshi, N., Baumann, M., Ehammer, A., Fensholt, R., Grogan, K., Hostert, P., ... & Reiche, J. (2016). A review of the application of optical and radar remote sensing data fusion to land use mapping and monitoring. Remote Sensing, 8(1), 70.

Lambin, E. F., Geist, H. J., & Lepers, E. (2003). Dynamics of land-use and land-cover change in tropical regions. Annual review of environment and resources, 28(1), 205-241.

Mora, O., Ordoqui, P., Iglesias, R., & Blanco, P. (2016). Earthquake Rapid Mapping Using Ascending and Descending Sentinel-1 TOPSAR Interferograms. Procedia Computer Science, 100, 1135-1140.

MultiSpectral Instrument (MSI) Overview. Sentinel Online. European Space Agency. Retrieved 3 December 2018.

Planet Team, Planet Application Program Interface: In Space for Life on Earth. San Francisco, CA, USA, 2017

Rosich, B., & Meadows, P. (2004). Absolute Calibration of ASAR Level 1 Products; ESA/ESRIN (No. 1). ENVI-CLVL-EOPG-TN-03-0010.

Small, D. (2011). Flattening gamma: Radiometric terrain correction for SAR imagery. IEEE Transactions on Geoscience and Remote Sensing, 49(8), 3081-3093.

Small, D., & Schubert, A. (2008). Guide to ASAR geocoding. ESA-ESRIN Technical Note RSL-ASAR-GC-AD, (1.01), 36.

Spoto, F., Sy, O., Laberinti, P., Martimort, P., Fernandez, V., Colin, O., ... & Meygret, A. (2012, July). Overview of Sentinel-2. In Geoscience and Remote Sensing Symposium (IGARSS), 2012 IEEE International (pp. 1707-1710). IEEE

Statistical Committee of the Republic of Armenia, Statistical information dissemination and public relations division of NS RA (2018)

Torres, R., Snoeij, P., Davidson, M., Bibby, D., & Lokas, S. (2012, July). The Sentinel-1 mission and its application capabilities. In Geoscience and Remote Sensing Symposium (IGARSS), 2012 IEEE International (pp. 1703-1706). IEEE.